Draft version October 18, 2021
Typeset using LaTeX default style in AASTeX63

p-Mode Oscillations in Gravitationally Highly Stratified Magnetic Solar Atmospheres

M. Griffiths,[1] R. Erdélyi,[2,3,4] R. Zheng,[5] and N. Gyenge[1]

[1] *Research IT, The University of Sheffield, 10-12 Brunswick Street, Sheffield, S10 2FN, UK.*
[2] *Solar Physics and Space Plasma Research Centre (SP^{2}RC), School of Mathematics and Statistics, University of Sheffield, Hicks Building, Hounsfield Road, S7 3RH, UK*
[3] *Department of Astronomy, Eötvös Loránd University, Pázmány P. sétány 1/A, Budapest, H-1117, Hungary*
[4] *Gyula Bay Zoltán Solar Observatory (GSO), Hungarian Solar Physics Foundation (HSPF), Petőfi tér 3., Gyula, H-5700, Hungary*
[5] *Shandong Key Laboratory of Optical Astronomy and Solar-Terrestrial Environment, School of Space Science and Physics, Institute of Space Sciences, Shandong University, Weihai, Shandong, 264209, China*

(Received June 1, 2019; Revised January 10, 2019; Accepted October 18, 2021)

Submitted to AJ

ABSTRACT

v4 after editorial request to remove duplication

The aim of the work reported in this paper is to gain understanding of the propagation characteristics of p-mode oscillations in the highly gravitationally stratified magnetic solar atmosphere. An objective is the measurement of the properties of the solar atmosphere and its magnetic structures. We present a comparison of the analysis of results from observations and numerical simulations.

The paper describes 3D numerical magnetohydrodynamic (MHD) simulations of a model solar atmosphere with a uniform vertical cylindrically symmetric magnetic field and employing simulation drivers resulting in oscillations which mimic the behaviour of p-mode oscillations. The simulations were run for different values of the magnitude of the magnetic field and a p-mode driver with a fixed period of 300 s. For the observational study, a typical active region was selected. We report results for the temporal analysis of the observational data for a region containing a small sunspot (solar pore).

The paper reports the variation of the energy flux and oscillation frequency of the magnetosonic modes and examines their dependence on the magnetic field strength. The comparison with observational data indicate the presence of oscillation signals with a frequency close to that measured for the simulated results.

We conclude that magnetic regions of the solar atmosphere are favourable regions for the propagation of energy by slow magnetosonic modes. The results exhibit a frequency shift, for different values of the magnetic field. The obtained periodic behaviour is confirmed by observational data, featuring similar frequencies based on the intensity times series of images taken by the Solar Dynamics Observatory.

Keywords: editorials, notices — miscellaneous — catalogs — surveys

1. INTRODUCTION

Theoretical and computational studies coupled with observations from solar telescopes reveal diverse structures and dynamics in the Sun's atmosphere. The culmination of these studies of the Chromosphere and the upper solar atmosphere has enhanced our knowledge of the variety of magnetic field structures. Despite our armoury of observations and the diverse range of computational models it still remains a challenge to make sense of this complex menagerie of dynamical structures, understand solar atmospheric heating (i.e. chromospheric and coronal) and more generally space weather phenomena.

Corresponding author: M. Griffiths
m.griffiths@sheffield.ac.uk

An example of the dynamical complexity are the ubiquitous five-minute oscillations in the solar atmosphere that are referred to as the solar global acoustic oscillations or p-modes. These global oscillations are interpreted as trapped acoustic waves, i.e. standing acoustic oscillations of the solar interior. Earlier models of these oscillations assumed that there was reflection by the photosphere with at most evanescent propagation above the photosphere. It has been realised that with kinetic pressure as the restoring force, acoustic oscillations of the photosphere may be perturbed by the solar p-modes. There is now increasing evidence for leakage of these modes. The p-modes were interpreted as resonant modes trapped in a cavity formed from the steep change in density at the solar surface and a lower turning point in the interior caused by the increase in the speed of sound resulting in refraction. The physical characteristics of the solar sub-surface layers can be estimated using observations of the standing modes.

The complexity and variety of magnetic structures in the solar atmosphere gives rise to a mixture of waves providing powerful diagnostics to aid our understanding and advance our knowledge. The characteristics of generated waves are dependent on the motions at the footpoints of magnetic field concentrations including those in the intergranular lanes. For example vortex motions have been demonstrated to generate Alfvén waves Fedun et al. (2009b).

In this paper, we report the results of numerical simulations of photospheric p-mode oscillations in a model solar atmosphere with a uniform and vertical magnetic field. First, we consider the variety of magnetic structures in the solar atmosphere and address the wave motions that are observed in these regions. This is followed with a description of the solar atmospheric model, magnetic field configuration and the simulation method we used to model p-mode oscillations in a model magnetic solar atmosphere.

2. STRUCTURES IN THE SOLAR ATMOSPHERE

There are many different kinds of structures in the highly dynamic solar chromosphere. Bright spots which form in the trenches between solar granules are known as faculae, these features which are formed near magnetic field concentrations constantly form and dissipate over time scales of several minutes. Pores are a few Mm across and they are the smaller counterparts of sunspots, they are the bright areas near to and around sunspots or faculae. The bright areas that extend away from active regions are called plage regions. The magnetic fields in this area diffuse away into the quiet Sun regions. The magnetic network is a network of lines which outline super-granules. Super-granules are convective regions about 30 Mm across, and they possess strong horizontal flows. The motions within the super-granules result in the concentration of bundles of magnetic field lines. The mean photospheric field in the inter-network region is 100-300 G. On the other hand, solar active regions contain sunspots which have sizes between 1 - 50 Mm.

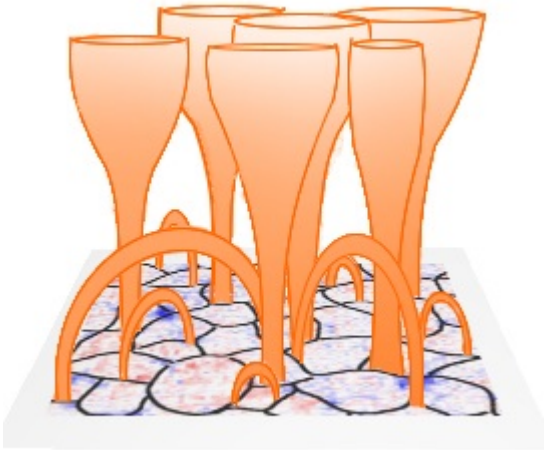

Figure 1. The schematic solar magnetic network.

Active regions producing flares may have fields which easily exceed the normal range of 100-500 G. As well as these massive concentrations, solar magnetograms reveal many north poles in the quiet photosphere, this is known as the

magnetic carpet. These structures can be observed in figure 1. Along with the coronal funnels arising from grain boundaries, the picture shows a range of network loops with temperatures which can be in the range 10^5K to 10^6K. The dynamical phenomena of concern in this paper result in waves and oscillations in the solar atmosphere. The upward propagation of waves through the solar atmosphere can result in coronal heating, frequency shifts and other wave phenomena. A range of wave transformations may occur including reflection and refraction by atmospheric structures.

Our initial computational studies were applicable to quiet sun regions regions with magnetic fluxes in the range 5-10G this includes the non magnetic solar chromosphere and the quiet inter-network regions between the magnetic flux concentrations. Given the variety of solar atmosphere regions for example the network, inter network, plage and faculae regions it is recognised that the modes of oscillation with periods of 3 and 5 minutes exhibit varying behaviour. In particular is the variation observed for different magnetic structures and reflecting layers such as the transition layer which influences propagation in the upward and downward direction.

The power spectra presented in the first figure of Griffiths et al. (2018b) exhibit a variation of propagation characteristics at different levels within the solar atmosphere and within different regions such as coronal holes, the quiet sun and active regions. In general the power spectra indicate a preponderance of long period 5 minute waves with frequencies in the range 1.5-5mHz. Also observed are the distinctive peaks for the short period 3 minute waves (with frequencies in the range 5-8mHz). The power spectra exhibit peaks in much longer period ranges for example 12 minute waves (frequencies in the range 1.1-1.5mHz) and 16 minute waves (frequencies 1-1.1mHz). For the quiet sun regions the 5 minute modes are stronger at photospheric levels and diminished higher up in the corona, but note a small peak for the data from the AIA 211 corresponding to 2.0MK.

The review of Khomenko and Calvo Santamaria (2013) summarises this multifaceted picture. In the close proximity of the magnetic network elements, the longer 5 minute modes propagate efficiently to the chromosphere. The 3 minute modes propagate from the photoshere to the chromosphere in the network cell interiors for restricted regions of the network and internetwork. Although these long-period halos are present in the chromosphere they are most prominent in the photosphere. With their more complex magnetic structures, a more complex pattern is exhibited in plage and faculae regions. Observations show that the 3 minute modes exhibit enhancement in both photosphere and chromosphere whereas the power of the 5 minute modes increase significantly in the chromosphere. These power enhancements are known as "halos" and have been widely reported Kontogiannis et al. (2010).

3. MOTIVATION

Given the complexity of the dynamics and the diversity of structures in the solar atmosphere, it is understood that a truly realistic model is challenging and requires a hybrid multi-disciplined approach. In order to develop a model providing a representation of the solar atmosphere it is necessary to establish that the modelling tools give a consistent behaviour in idealised test cases and that there is a consistency between the computational and theoretical models. Many computational MHD simulations of the sun have been undertaken, some of the approaches have resulted in an encouraging degree of realism Vögler et al. (2005), Gudiksen et al. (2011). Computational MHD simulations of the propagation of waves in 3D solar atmospheres were undertaken by Fedun et al. (2009a). Initially they considered hydrodynamical models, in later simulations Fedun et al. (2009b) Vigeesh et al. (2012) reported results for magnetized solar atmospheres featuring an idealized flux tube. These models with point drivers demonstrated the leakage of magneto-acoustic energy into the solar atmosphere. The work of Khomenko and Calvo Santamaria (2013) and Calvo Santamaria, Khomenko and Collados (2015) reviewed and presented 2D computational MHD modelling of wave propagation in magnetic features such as sunspots and arcades.

The models reveal that vertical magnetic fields enable energy to reach the corona. Our initial models of a realistically stratified model of the solar atmosphere Griffiths et al. (2018b) were hydrodynamic simulations. In these simulations atmospheric perturbations caused by photospheric global oscillations are represented using drivers located in the photosphere so as to mimic the influence of the solar p-modes. The results of the hydrodynamic modelling exhibited agreement with the energy flux predictions from a 2 layer Klein-Gordon model. This agreement supported the interpretation of the interaction between the solar atmosphere and the global oscillations. Also revealed by the simulations was a consistency between power flux measurements from SDO and frequency dependent energy flux measurements from the numerical simulations. This observed propagation of energy into the mid to upper atmospheric regions of the quiet sun occurred for a range of frequencies. Such observations may explain observed intensity oscillations for periods

greater than the well known 5-minute and 3-minute oscillations. It was also found that energy flux propagation into the lower solar corona is strongly dependent on the particular wave modes.

In this paper we present results for 3D numerical MHD simulations with an extended driver representing photospheric p-mode oscillations in a magnetic solar atmosphere, the objective is to gain understanding of the propagation characteristics of the p-mode oscillations.

4. NUMERICAL COMPUTATION METHODS

The simulations described in in this paper were undertaken using the SMAUG code, a GPU implementation of the Sheffield Advanced Code (SAC) Shelyag et al. (2008). The Sheffield MHD Accelerated Using GPUs (SMAUG) Griffiths et al. (2015) and SAC are derived from the versatile advection code (VAC) developed by (Tóth 1996). SAC and SMAUG are numerical MHD solvers which can be used to model the time-dependent evolution of photospheric oscillations in the solar atmosphere. The SMAUG code can simulate linear and non-linear wave propagation in strongly magnetised plasma with structuring and stratification.

We use the same general system of ideal MHD equations applicable to an ideal compressible plasma and used for the hydrodynamic simulations Griffiths et al. (2018b).

$$\frac{\partial \rho}{\partial t} + \nabla \cdot (\rho \mathbf{v}) = 0, \tag{1}$$

$$\frac{\partial (\rho \mathbf{v})}{\partial t} + \nabla \cdot (\mathbf{v}\rho\mathbf{v} - \mathbf{B}\mathbf{B}) + \nabla p_t = \rho \mathbf{g}, \tag{2}$$

$$\frac{\partial e}{\partial t} + \nabla \cdot (\mathbf{v}e - \mathbf{B}\mathbf{B} \cdot \mathbf{v} + \mathbf{v}p_t) + \nabla p_t = \rho \mathbf{g} \cdot \mathbf{v}, \tag{3}$$

$$\frac{\partial \mathbf{B}}{\partial t} + \nabla \cdot (\mathbf{v}\mathbf{B} - \mathbf{B}\mathbf{v}) = 0. \tag{4}$$

The total pressure p_t is given by

$$p_t = p_k + \frac{\mathbf{B}^2}{2}, \tag{5}$$

and the kinetic pressure, p_k, is written as

$$p_k = (\gamma - 1)\left(e - \frac{\rho \mathbf{v}^2}{2} - \frac{\mathbf{B}^2}{2}\right). \tag{6}$$

In the system of equations above, $\mathbf{B}$ is the magnetic field, $\mathbf{v}$ is the velocity, ρ is the mass density, $\mathbf{g}$ is the gravitational acceleration vector and e is the energy density. The SMAUG code used for the simulations reported here employs perturbed versions of the general set of MHD equations given above. For the perturbed versions the density, energy density and magnetic field are expressed in terms of perturbed and background quantities as follows

$$\rho = \tilde{\rho} + \rho_b,$$
$$e = \tilde{e} + e_b,$$
$$\mathbf{B} = \tilde{\mathbf{B}} + \mathbf{B}_b.$$

Assuming a magneto-hydrostatic equilibrium of the background plasma, the background quantities which do not change in time have a subscript b. The time varying perturbed quantities do not have a subscript. The fully non-linear MHD numerical finite element solver employs hyper-diffusion and hyper-resistivity to achieve numerical stability of the computed solution of the MHD equations Caunt and Korpi (2001). A more detailed description of the full set of MHD equations, including the hyper-diffusion source terms are given in Griffiths et al. (2015) and Shelyag et al. (2008).

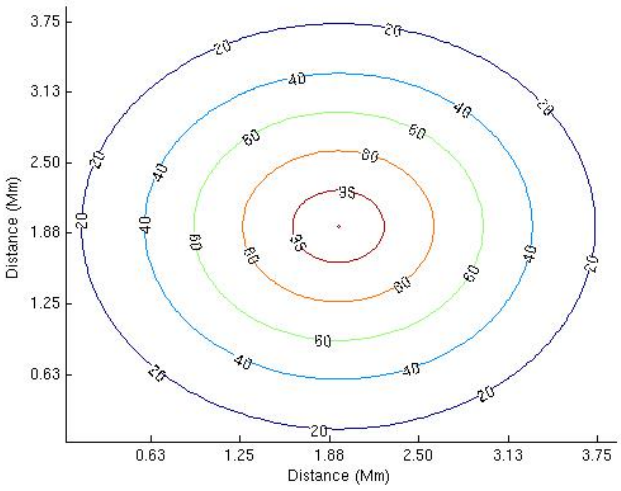

Figure 2. Initial Magnetic Field Configuration, radial field distribution, uniform in the vertical direction with a maximum value of 100G

5. COMPUTATIONAL MODEL

The hydrodynamical studies reported in Griffiths et al. (2018b) employed simulation drivers with physical characteristics representing p-mode oscillations with varying modes and periods. The MHD simulations reported here used a model of the solar atmosphere and included a uniform vertical cylindrically symmetric magnetic field.

The dimensions of the simulation box are $L_x = 4$ Mm, $L_y = 4$ Mm and with a height of $L_z = 6$ Mm in the gravitationally stratified z-direction. The computational box is an array of elements $128 \times 128 \times 128$. The upper boundary of the model is in the solar corona whilst the lower boundary is coincident with the photosphere. The perturbed MHD code used here is suited to studying the propagation of wave energy from the photosphere, across the transition layer and leaking into the solar corona. The time scales relevant to our study are determined by the 5-minute p-mode oscillations the model employs open boundary conditions thereby allowing us to model the wave propagation. To generate these oscillations we use vertical velocity drivers which are extended across the base of the model. The following sections describe the model solar atmosphere and the driver.

Data obtained from solar observations was used to construct a semi-empirical model solar atmosphere, the resulting model is a representation of the quiet sun. Employing the fundamental assumption of hydrostatic equilibrium, the VALIIIc model Vernazza et al. (1981) was used to construct a model of the chromosphere in equilibrium. For atmospheric heights greater than 2.5 Mm the results from a model of solar coronal heating were used (see McWhirter et al. 1975). A further possiblity for a model solar atmosphere is the use of parametric models, the smoothed step function used by Murawski and Zaqarashvili (2010) is an example. Discussion of the validity of model solar atmospheres and realistic models of the chromosphere, indicate the need for observationally derived semi-empirical models, see Carlsson and Stein (1995), Kalkofen (2012). It has been suggested that local dynamo action and joule heating in the dynamical solar chromosphere make the construction of models particularly challenging Leenaarts et al. (2011).

For the simulations described here we use a simplistic model which is uniform in the vertical (z) direction. The cylindrically symmetric field was constructed using the parametrisation in equation 7, the effective cylinder radius was fixed at $R = 0.14Mm$. Simulations were run for different values of B_{max}.

$$B_z = B_{max} e^{-\frac{x^2+y^2}{R^2}}, \tag{7}$$

Since the field is uniform in the vertical direction the model atmosphere in hydrostatic equilibrium is in magnetohydrostatic equilibrium. Details of the construction procedure for the model atmosphere, the resulting density profiles and temperature profiles are provided in Griffiths et al. (2018b).

6. NUMERICAL DRIVERS FOR P-MODE OSCILLATIONS

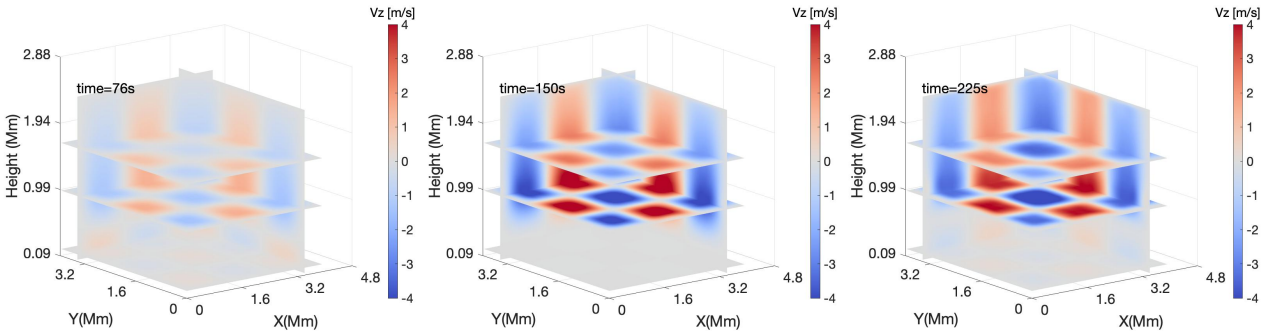

Figure 3. Vertical Component of the Velocity for Different Sections of the Simulation for 76s, 150s and 225s for a vertical field with maximum field of 100G.

The work reported here is an extension of the earlier work of Malins (2007), their study represented photospheric buffeting motion using different point drivers. These studies demonstrated surface waves, structures in the transition zone and identified the effect of cut-offs induced by the stratified solar atmosphere. The overview in Section 2 identified physical phenomena delivering energy into the solar atmosphere and resulting in oscillatory behaviour.

The simulations presented in this paper, employ an extended driver resulting in the perturbation of the entire lower boundary of the model. Photospheric p-mode oscillations for the real sun have a horizontal wavelength and coherence. The vertical velocity driver used here is an acoustic p-mode driver located at the photosphere and exciting waves which propagate into our realistic 3D model of the solar atmosphere. An extended driver with a sinusoidal dependence and a wavelength of 8 Mm applied along the middle of the base of a computational domain of dimension 4 Mm represents a *fundamental mode*. Drivers may be constructed as an ensemble of these solar global eigenmodes. The driver is represented by the expression shown in equation (8)

$$V_z = A_{nm} \sin\left(\frac{2\pi t}{T_s}\right) \sin\left(\frac{(n+1)\pi x}{L_x}\right) \sin\left(\frac{(m+1)\pi y}{L_y}\right) \exp\left(-\frac{(z-z_0)^2}{\Delta z^2}\right), \tag{8}$$

For the simulations here, a p-mode driver corresponding to the 5 minute mode, was used with period 300s and mode (2,2). Earlier studies demonstrated the effectiveness of this mode with energy propagation. Simulations were run for different values of the magnitude of the magnetic field. The mode numbers identified here are the n and m values in the expression for the driver shown in equation (8).

For the driver equation given in 8, T_s is the period, A_{nm} is the amplitude, the indices n and m define the mode, the lengths of the base of the simulation box in the x and y directions are L_x and L_y are respectively. The driver width, Δz is set to $4km$, the parameter z_0 was set so that the vertical location of the driver is in the photosphere, coincident with the location of the temperature minimum and 0.5 Mm above the lower boundary of the model. The simulations presented use the parameter A_{nm}=500 ms^{-1} with the mode indices set to $n, m = 2$.

7. MAGNETOACOUSTIC WAVES IN UNIFORM VERTICAL MAGNETIC FIELD CONFIGURATIONS

Magnetohydrodynamic simulations have been performed with p-mode oscillations of the photospheric layer and for magnetic field strengths of 0G, 50G, 75G and 100G. The plasma β for the model decreases rapidly from a value of 12 at the lower boundary of the simulation domain, β decreases to 1 at a height of 0.5Mm. From the top of the transition layer to the upper boundary of the model β has a constant value of 1×10^{-6}. It is anticipated that for the region with $\beta \approx 1$, mode conversion occurs with full or partial conversion to magnetohydrodynamic modes.

Figure 3 shows the vertical component of the velocity at various times for different sections through the simulation box. Each plot in figure 3 corresponds to a vertical field configuration with a maximum field strength (B_{max}) of 100G. Referring to Griffiths et al. (2018b), there is a clear difference between the purely hydrodynamic, 0G case and the MHD cases. The figures exhibit evidence of a fast moving magneto-acoustic wave mode. These figures compare the wave modes at a quarter, half and three-quarters of a cycle. The propagation speed is consistent with that of a fast magneto-acoustic mode. Our results indicated that even a small magnetic field appears to enhance the motion of plasma in the corona and there is an apparent difference in phase between the magnetic field cases. As well as an increase in the velocity amplitude with increasing magnetic field there is a small shift in the frequency of the oscillation. For magnetic fields with strengths between $1kG$ and$50G$, the theoretical prediction of Hindman et al. (1996) resulted

Wave Speed (km/s)	0G	50G	75G	100G
2Mm	12.6	96.5	47.7	25.2
1Mm	10.1	64.1	44.4	45.4
0.5Mm	8.7	45.4	37.8	32.3

Table 1. The table shows wave speeds obtained from the distance-time plots for the 300s period driver with magnetic fields of 0G,50G, 75G and 100G.

Magnetic Field (G)	1Mm	2Mm	4Mm	5.5Mm
0G	0.2625	0.0021	1.4846×10^{-6}	1.7399×10^{-6}
50G	0.5401	-4.9441	0.882	0.5417
75G	0.1978	-1.576×10^{-4}	1.1586×10^{-6}	8.1936×10^{-7}
100G	0.0165	-1.8664	0.7116	0.4092

Table 2. The table shows the time averaged and integrated energy flux ratio obtained for the 300s period driver with magnetic fields of 0G,50G, 75G and 100G.

in frequency shifts in the microhertz and nanohertz range, although this was a helioseismology prediction it provides insight into the mechanism of frequency shifts of waves in atmospheric magnetic structures.

A set of videos of all the simulations that were performed can be obtained from the online research data archive hosted by The University of Sheffield Griffiths et al. (2018a). The videos display the evolution of the z-component of the plasma velocity along different layers of our model solar atmosphere. Each video shows the value of the vertical component of the plasma velocity (z-component in m/s) along different slices through the simulation box. Each video is labelled using the magnetic field strength in Gauss.

A distance-time plot for the 300s period driver, with the 100G field is shown in figure 4. The wavespeeds computed from this distance-time plot are shown in table 1. The speeds for the 0G field are consistent with the speed of sound in the solar atmosphere, whilst the speeds for the non zero magnetic field are consistent with propagation speeds for magnetosonic modes.

In the lower region of the model atmosphere the simulations exhibit evidence of slow magnetoacoustic wave propagation perpendicular to the field lines. Since the source terms perturb only the vertical component of the velocity and the model is cylindrically symmetric, pure Alfvenic modes are not expected.

To investigate the influence of the magnetic field on the propagation of wave energy we employ an expression for the energy flux which was used by Bogdan et al. (2003). The wave energy flux $\mathbf{F_{wave}}$ is given by

$$\mathbf{F}_{wave} = \tilde{p}_k \mathbf{v} + \tilde{\mathbf{B}} \cdot \mathbf{B}_b \mathbf{v} + \mathbf{v} \cdot \tilde{\mathbf{B}} \mathbf{B}_b.$$

We compute the time averaged energy flux integrated over different cross sections of the simulation box.

$$F_{int} = \frac{1}{t_{max}} \int_0^{t_{max}} \int \mathbf{F}_{wave} \cdot d\mathbf{A} dt, \tag{9}$$

These expression are dependent on the perturbed kinetic pressure $\tilde{p}_k$.

$$\tilde{p}_k = (\gamma - 1) \left(\tilde{e} - \frac{(\tilde{\rho} + \rho_b) \mathbf{v}^2}{2} - \frac{\mathbf{B}^2}{2} \right).$$

Using equation (9), we computed the energy flux integral for each of the drivers at different atmospheric heights and averaged over the total time. We compute the ratio of this integrated energy flux to the integrated energy flux at the location of the driver, the resulting values are shown in table 2 . With the exception of the 75G field case it appears that the energy flux is enhanced for increasing values for the vertical magnetic field. In figure 5 we plot the ratio of the integrated energy flux ratio for different values of the field at different heights and for the different vertical field values (the blue, orange and red are for field values of 50G, 75G and 100G respectively). This plot demonstrates that for higher B-field magnitudes the energy propagation is suppressed, this is interesting because this is consistent with observations and other simulation results which demonstrate an enhancement for inclined fields.

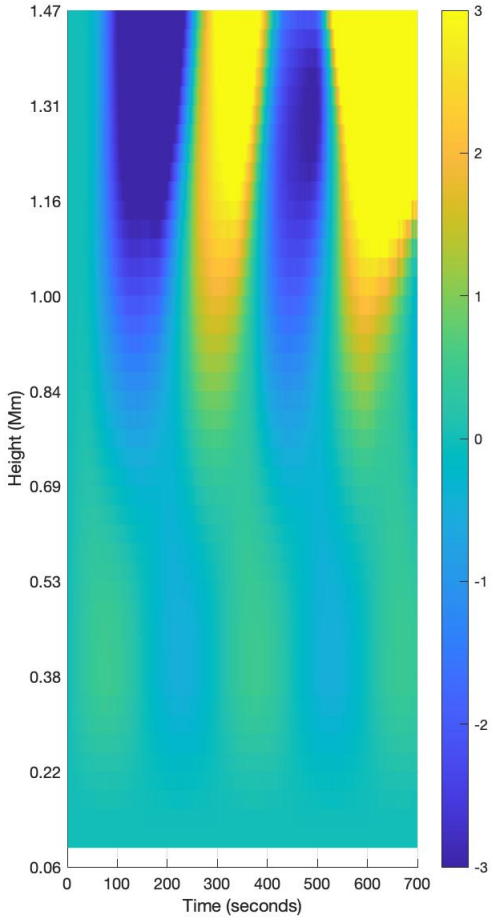

Figure 4. Distance-time plot of the vertical component of the velocity in the mid chromosphere.

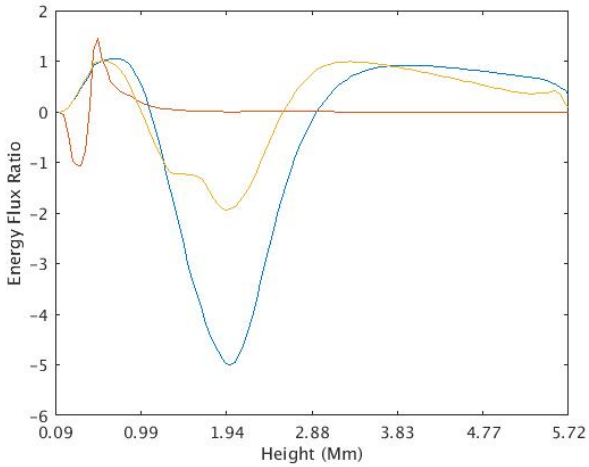

Figure 5. Shows the Ratio of the Integrated Energy Flux ratio for different values of the field, Blue 50G, Orange 75G, Red 100GMm

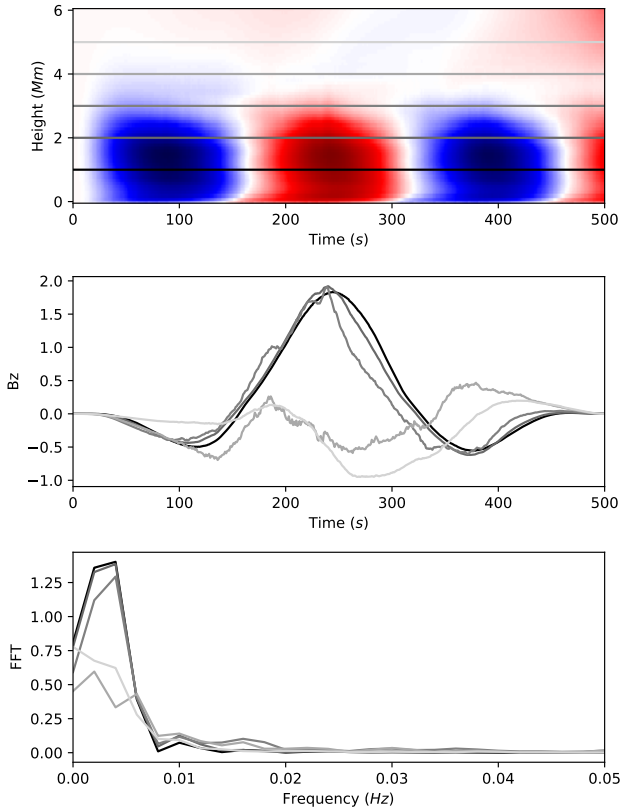

Figure 6. Temporal analysis of Bz vertical slices at 2 Mm. The top panel shows the selected vertical slices, indicated by gray colours. The middle panel demostrates the obtained signal after applying a Hanning window function. The bottom panel shows the result of the FFT analysis based on the 5 selected vertical Bz slices.

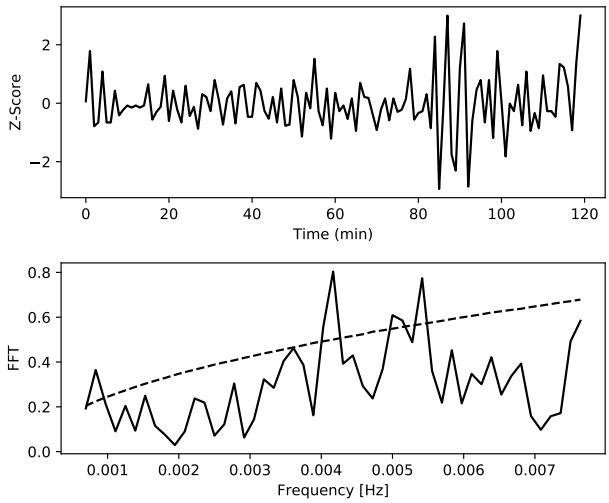

Figure 7. Temporal analysis of pixel intensity based on AIA 1600Å between 18:00 UT to 20:00 UT on 22 August 2010. The upper panel shows the temporal variation of the Z-Score (detrended and normalised pixel intensity data). The lower panel shows the FFT of the analysed observational data.

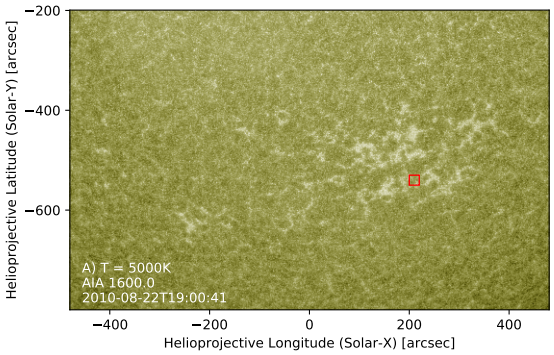

Figure 8. The selected pixel from the start of the investigate time series at 18:00 UT on 22 August 2010. The pixel is indicated by red rectangle.

8. FREQUENCY ANALYSIS

The top panel of Figure 6 shows a vertical slice of Bz over time, this is based on the simulation with the initial magnetic field configuration with a maximum value of 100 G. The vertical axis represents the height in Mm and the horizontal axis is the time dimension, measured in seconds. From this 2-dimensional plane, we selected 5 layers, indicated by vertical grey lines. The middle panel of Figure 6 displays the temporal variation of the selected layers, indicated by different grey shade colours. The time series do not feature non-stationary behaviour, therefore, further transformations (such as de-trending, smoothing or differentiation) are not needed. The Hanning-window function is still applied to avoid leakage effects when performing the Fast Fourier Transformation (FFT).

An FFT is applied (the lower panel) for investigating any oscillatory behaviour in the analysed signal. A significant oscillatory pattern is found with frequency range of 3.75 - 4 mHz, corresponding a period range of 4.2 - 4.4 minutes. FFT was also performed based on other simulations with different initial magnetic field configurations (with a maximum value of 0 G, 50 G 75 G and 100 G). These investigations all showed similar oscillatory behaviour, therefore, we present one FFT as a representative example.

Next, temporal analysis for observational data is performed for confirming the obtained oscillatory behaviour. We investigate intensity oscillations in the solar atmosphere observed by SDO/AIA. The passband 1600 Å is selected because our simulation mainly focuses on lower atmospheric regions, i.e. photosphere and chromosphere. The cadence of 1600 Å images is 24 seconds, therefore it is suitable for studying relatively high-frequency oscillations such as the obtained 4 mHz.

The initial magnetic field configuration of our model is a standing magnetic tube, passing through the chromosphere and the lower corona. Therefore, We chose to sample a typical active region. The selected area contains a small sunspot (solar pore), presumably featuring similar magnetic structure as our simulation. From each observation, a single pixel is selected, yielding a 0.35 Mm by 0.35 Mm area. The obtained time series shows non-stationary behaviour, therefore, the observed linear trend is removed by taking the first difference Δy_t of the data. The first difference is defined as the difference between consecutive observations y_t and y_{t-1}. Furthermore, the times series is also normalised by applying standard scores (Z-scores), defined by:

$$Z_i = \frac{T_i - \overline{T}}{\sigma(T)}, \tag{10}$$

where, the parameter $\overline{T}$ is the mean of the time series and the parameter $\sigma(T)$ is defined as the standard deviation of the data. The top panel of Figure 6 demonstrates the trend removed and normalised time series. The lower panel of Figure 6 shows the result of the applied FFT technique. The dashed line is the significance level (3σ) which is calculated by Monte-Carlo method. The original data showed red noise signature which transformed to blue noise after differentiating the data. We have generated 1 million blue noise signatures N_b and calculated the standard deviation $\sigma(N_b)$ and the mean $\overline{N_b}$ of the simulated noise, providing our significance level S:

$$S = \overline{N_b} + 3\sigma(N_b). \tag{11}$$

A significant period is found with frequency range of $4 - 4.2\ mHz$, corresponding a period range of 4 - 4.2 minutes, which is close to the period found in simulation data. Another significant peak is found with period around 3 minutes which may be an indication of another global oscillation.

9. CONCLUSION

In this paper we have presented results for a series of MHD simulations of an extended oscillator at the base of a model solar atmosphere. We have shown that energy is propagated by magnetosonic modes. Slow and fast magnetosonic modes are responsible for carrying some energy back to the chromosphere and the photosphere. The results exhibit a small frequency shift for different values of the magnetic field closer inspection of the energy flux propagation results indicative of enhanced energy flux propagation for inclined magnetic fields. The obtained periodic behaviour is confirmed by observational data, featuring similar frequencies based on the intensity times series of SDO images. The frequency shift measured from the temporal analysis of the observational and simulation data is larger than would be expected from the analysis of Hindman et al. (1996). This can be understood in part by referring to the work of Campbell and Roberts (1989).

It is encouraging that the results presented here are consistent with the behaviour exhibited by earlier work. Future work will address simulation runs over longer time periods and for inclined fields. There is an issue that due to the extended nature of the driver the amplitudes used may be responsible for delivering vast quantities of energy into the solar atmosphere and for driving a highly numerically unstable system and inducing extremely large shocks Calvo Santamaria, Khomenko and Collados (2015).

10. ACKNOWLEDGMENTS

The authors thank P. H. Keys for providing the wavelet tools to analyse the related SDO data M.Korsos for the preparation of Figure 1, the Science and Technology Facilities Council (STFC) for the support they received. RE acknowledges the support received from the the Royal Society (UK). We acknowledge IT Services at The University of Sheffield for the provision of the High Performance Computing Service.

Software: SMAUG (Griffiths et al. 2015), SAC (Shelyag et al. 2008), VAC (Tóth 1996)

REFERENCES

Bogdan, T. J., Carlsson, M., Hansteen, V. H., McMurry, A., Rosenthal, C. S., Johnson, M., Petty-Powell, S., Zita, E. J., Stein, R. F., McIntosh, S. W., Nordlund, Å., 2003. Waves in the Magnetized Solar Atmosphere. II. Waves from Localized Sources in Magnetic Flux Concentrations. ApJ599, 626–660.

Calvo Santamaria, I., Khomenko, E., and Collados, M., 2015. Magnetohydrodynamic wave propagation from the subphotosphere to the corona in an arcade-shaped magnetic field with a null point. A&A577, A70.

Campbell, W. R. and Roberts, B. 1989. The Influence of a Chromospheric Magnetic Field on the Solar p- and f-Modes ApJ, 338, 538. doi:10.1086/167216

Carlsson, M., Stein, R. F., 1995. Does a nonmagnetic solar chromosphere exist? ApJL440, L29–L32.

Caunt, S. E., Korpi, M. J., Apr. 2001. A 3D MHD model of astrophysical flows: Algorithms, tests and parallelisation. A&A369, 706–728.

Fedun, V., Erdélyi, R., Shelyag, S., Sep. 2009. Oscillatory Response of the 3D Solar Atmosphere to the Leakage of Photospheric Motion. SoPh258, 219–241.

Fedun, V., Erdélyi, R., Shelyag, S., Sep. 2009. MHD waves generated by high-frequency photospheric vortex motions. Annales Geophysicae 29, 1029-1035.

Griffiths, M. K., Fedun, V., Erdélyi, R., 2015. A Fast MHD Code for Gravitationally Stratified Media using Graphical Processing Units: SMAUG. Journal of Astrophysics and Astronomy 36, 197–223.

Griffiths, M., Erdélyi, R., Fedun, V., 2017. Videos of Magnetohydrodynamics Simulations of Solar Atmosphere Wave Dynamics Generated by Solar Global Oscillating Eigenmodes. https://figshare.com/articles/Videos_of_Magnetohydrodynamics_Simulations_of_Solar_Atmosphere_Wave_Dynamics_Generated_by_Solar_Global_Oscillating_Eigenmodes/4818490

Griffiths, M., Erdélyi, R., Fedun, V., 2018. Videos of p-Mode Oscillations in Highly Gravitationally Stratified Magnetic Solar Atmospheres. https://figshare.com/articles/Videos_of_Magnetohydrodynamics_Simulations_of_Solar_Atmosphere_Wave_Dynamics_Generated_by_Solar_Global_Oscillating_Eigenmodes/4818490

Griffiths, M. K., Fedun, V., Erdélyi, R., and Zheng,R., Solar atmosphere wave dynamics generated by solar global oscillating eigenmodes.Advances in Space Research, 61: 720–737, January 2018.

B. V. Gudiksen, M. Carlsson, V. H. Hansteen, W. Hayek, J. Leenaarts, and J. Martínez-Sykora. The stellar atmosphere simulation code Bifrost. Code description and validation. *A&A*, 531:A154, July 2011. https://doi.org/10.1051/0004-6361/201116520.

Hindman, B. W. and Zweibel, E. G. and Cally, P. S., Mar. 1996. Driven Acoustic Oscillations within a Vertical Magnetic Field. ApJ459, 760–772.

Kalkofen, W., 2012. The Validity of Dynamical Models of the Solar Atmosphere. SoPh276, 75–95.

Khomenko, E., Calvo Santamaria, I., 2013. Magnetohydrodynamic waves driven by p-modes. Journal of Physics Conference Series 440 (1), 012048.

I. Kontogiannis, G. Tsiropoula, and K. Tziotziou. Power halo and magnetic shadow in a solar quiet region observed in the Hα line. *A&A*, 510:A41, February 2010. https://doi.org/10.1051/0004-6361/200912841.

Leenaarts, J., Carlsson, M., Hansteen, V., Gudiksen, B. V., 2011. On the minimum temperature of the quiet solar chromosphere. A&A530, A124.

Leighton, R. B., 1960. In: Thomas, R. N. (Ed.), Aerodynamic Phenomena in Stellar Atmospheres. Vol. 12 of IAU Symposium. pp. 321–325.

Malins, C., 2007. On transition region convection cells in simulations of {p}-mode propagation. Astronomische Nachrichten 328, 752–755.

McWhirter, R. W. P., Thonemann, P. C., Wilson, R., 1975. The heating of the solar corona. II - A model based on energy balance. A&A40, 63–73.

Murawski, K., Zaqarashvili, T. V., 2010. Numerical simulations of spicule formation in the solar atmosphere. A&A519, 9.

Shelyag, S., Fedun, V., Erdélyi, R., 2008. Magnetohydrodynamic code for gravitationally-stratified media. A&A486, 655–662.

Tóth, G., 1996. A General Code for Modeling MHD Flows on Parallel Computers: Versatile Advection Code. Astrophysical Letters and Communications 34, 245.

Vernazza, J. E., Avrett, E. H., Loeser, R., 1981. Structure of the solar chromosphere. III - Models of the EUV brightness components of the quiet-sun. Astrophysical Journal Supplement Series 45, 635–725.

Vigeesh, G.,Fedun, V.,Hasan, S. S., Erdélyi, R., Jan. 2012. Three-dimensional Simulations of Magnetohydrodynamic Waves in Magnetized Solar Atmosphere. ApJ755, 1–18.

A. Vögler, S. Shelyag, M. Schüssler, F. Cattaneo, T. Emonet, and T. Linde. Simulations of magneto-convection in the solar photosphere. Equations, methods, and results of the MURaM code. *A&A*, 429: 335–351, January 2005. https://doi.org/10.1051/0004-6361:20041507.